Basin-Scale Topographic Waves in the Gulf of Riga*

Urmas Raudsepp[+]

Estonian Marine Institute, Tallinn, Estonia

Dmitry Beletsky

Department of Naval Architecture and Marine Engineering, University of Michigan, Ann Arbor, Michigan

David J. Schwab

NOAA/Great Lakes Environmental Research Laboratory, Ann Arbor, Michigan

(Manuscript received 8 May 2001, in final form 18 November 2002)

ABSTRACT

A two-dimensional circulation model has been used to test the hypothesis of whether the observed low-frequency current variations in the central Gulf of Riga, Baltic Sea, can be explained by basin-scale topographic wave response. A comparison of two-dimensional model results with measurements from a single current meter in the gulf showed good correlation. More sophisticated three-dimensional barotropic and baroclinic models provided only marginal improvement over the two-dimensional model. The model results indicate that wind-driven flow over variable bottom topography is the dominant process during moderate and strong winds. The double-gyre circulation pattern resembles the gravest basin-scale topographic wave. The free topographic wave propagates cyclonically around the basin, but does not complete a full cycle because of the shallowness of the Gulf of Riga. The evolution of the topographic wave under realistic wind conditions is analyzed using vorticity dynamics in a basin-scale sense. The topographic wave is reinforced by cyclonically rotating wind and can be destroyed most effectively by anticyclonically rotating wind. The topographic wave signature is more apparent in deep water and almost absent in shallow areas of the basin. During calm periods or under the influence of weak winds, the double-gyre circulation will evolve into predominantly cyclonic circulation.

1. Introduction

The barotropic circulation in large lakes and enclosed seas driven by spatially uniform wind, which is often a reasonable approximation, is characterized by downwind currents at the coast and return flow in the center (deep part) of the basin (Bennett 1974). The spatial structure of the flow (double-gyre circulation) corresponds to the first mode basin-scale topographic wave (Lamb 1932; Ball 1965) and has been predicted by analytical solutions for many different depth profiles (e.g., Stocker and Hutter 1987). Under the influence of rotation this pattern will propagate slowly (with a frequency considerably less than inertial frequency) counterclockwise in the Northern Hemisphere (Csanady

Corresponding author address: Dr. Urmas Raudsepp, Estonian Marine Institute, Paldiski Rd. 1, Tallinn 10137, Estonia.
E-mail: raudsepp@online.ee

1974). If the wind stress is removed after the initiation of the flow and bottom stress is neglected, the double-gyre structure will propagate around the basin as a free topographic wave, with a period that depends on basin geometry and bathymetry (Saylor et al. 1980).

In natural basins with irregular topography, the basin-scale topographic waves may have far more complex spatial structure than predicted by analytical models (Rao and Schwab 1976). Also, the basin-scale topographic wave, once generated by a strong wind impulse, is influenced by subsequent wind events, altered by depth variations, and modified by friction and nonlinear effects. There is some evidence from numerical model experiments that the basin-scale double-gyre topographic wave is excited in a natural basin, and that the wave persists after wind forcing ceases or changes direction. Simons (1975) showed that storm-generated topographic modes evolve in accordance with the theory of free topographic waves in Lake Ontario for several days. His simulation was made for the case of a stratified lake, but the same results should apply to a homogeneous lake. Schwab (1983) simulated the topographic mode in Lake Michigan driven by an idealized oscillatory wind. Simons (1983)

addressed the problem of variable wind effect on topographic waves in a closed basin, but with the main emphasis on wave response in the coastal area. The dynamics of basin-scale topographic waves has mainly been studied with the linear vorticity equation for depth-averaged flow in the f plane, but Simons (1986) showed that the double-gyre structure will evolve into a predominant cyclonic vortex under the influence of weak winds because of nonlinear topographic wave interactions.

There are not very many cases in which current observations have sufficient spatial coverage to resolve the basin-scale topographic wave structure. Intensive measurements in southern Lake Michigan by Saylor et al. (1980) showed strong oscillatory currents over the central deep area of the lake, which were explained as basin-scale topographic waves. Recent observations have shown energetic low-frequency cyclonic rotation of the velocity vector in the near-bottom layer of the central Gulf of Riga, Baltic Sea. It was suggested that this was due to topographic wave response (Raudsepp and Kõuts 2001). We will test this hypothesis in the present study by applying a series of numerical models of various complexity to the Gulf of Riga. The Gulf of Riga is a relatively closed, almost circular eastern subbasin of the Baltic Sea (Fig. 1). It has two openings—the Irbe Strait (with a sill depth of 25 m and a minimum cross-section area of 0.4 km^2) in the west and the Virtsu Strait (with a sill depth of 5 m and a minimum cross-section area of 0.04 km^2) in the north. The gulf has a surface area of 14 000 km^2, a volume of 408 km^3, a mean depth of 29 m, and a maximum depth of 55 m. In this study, the Gulf of Riga is modeled as a closed basin.

The numerical models are described in section 2. The basin-scale circulation in the Gulf of Riga initiated by impulsive wind and its unforced evolution for linear and nonlinear models are discussed in section 3. Simulated currents for different levels of model sophistication are compared with measurements in section 4. The model results are analyzed for basin-scale vorticity dynamics, for rotating wind, and for weak wind in section 5. Conclusions are presented in section 6.

2. Numerical models

The numerical model adapted for the Gulf of Riga is based on the three-dimensional (3D) Princeton Ocean Model (Blumberg and Mellor 1987) and is a nonlinear, hydrostatic, primitive equation, finite-difference model with the Mellor and Yamada (1982) level-2.5 turbulence closure parameterization. The boundary condition for an enclosed basin is that there is no flow normal to the shoreline. The model uses time-dependent wind stress at the surface, free-slip lateral boundary conditions and a quadratic bottom friction. The model was mostly used in the two-dimensional (2D) mode (a shallow-water model), while 3D calculations were conducted as sensitivity studies. The bottom drag coefficient in the 2D model was 0.0025, horizontal diffusion was 50 m^2 s^{-1}.
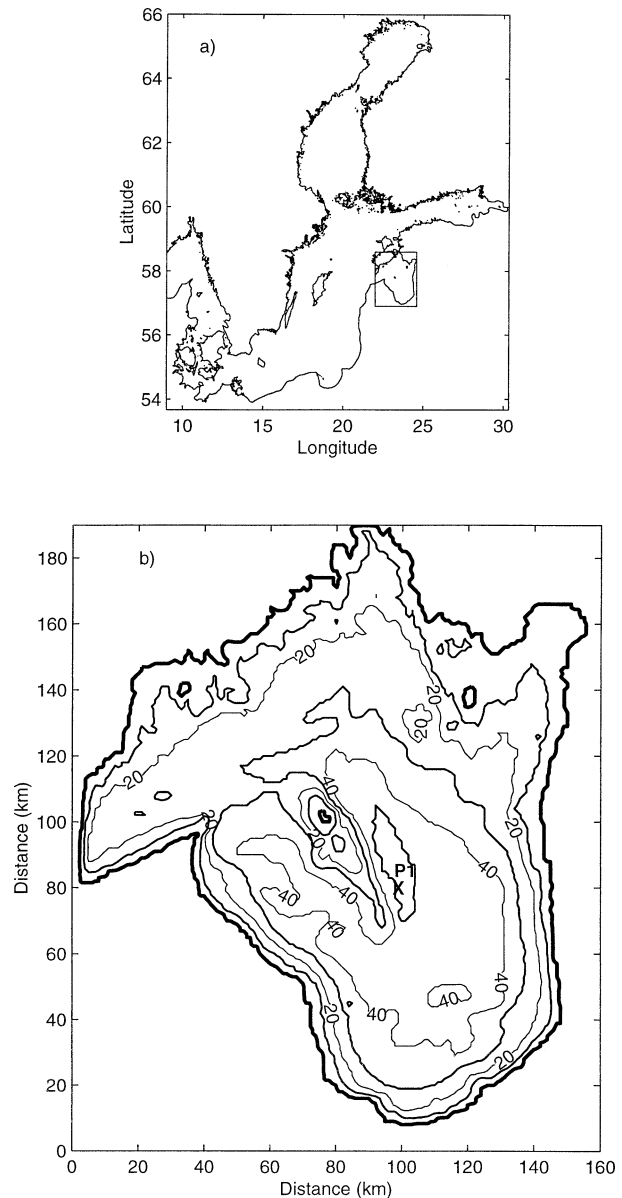

FIG. 1. (a) Map of the Baltic Sea and (b) bottom topography of the Gulf of Riga. The contour interval for the Gulf of Riga is 10 m and thicker lines corresponds to each 20 m. Point P1 corresponds to the location of the measurements.

Comparison with 3D model results and observations indicated that these values provide reasonable results. In the 3D model, the drag coefficient in the bottom friction formulation is spatially variable. It is calculated based on the assumption of logarithmic bottom boundary layer using constant bottom roughness of 0.01 m. Horizontal diffusion is calculated with a Smagorinsky eddy parameterization (Smagorinsky 1963). To examine the dynamics of basin-scale topographic waves in an idealized setting, a linearized version of 2D Princeton Ocean Model will also be used. In this model horizontal advection and diffusion is neglected and bottom friction
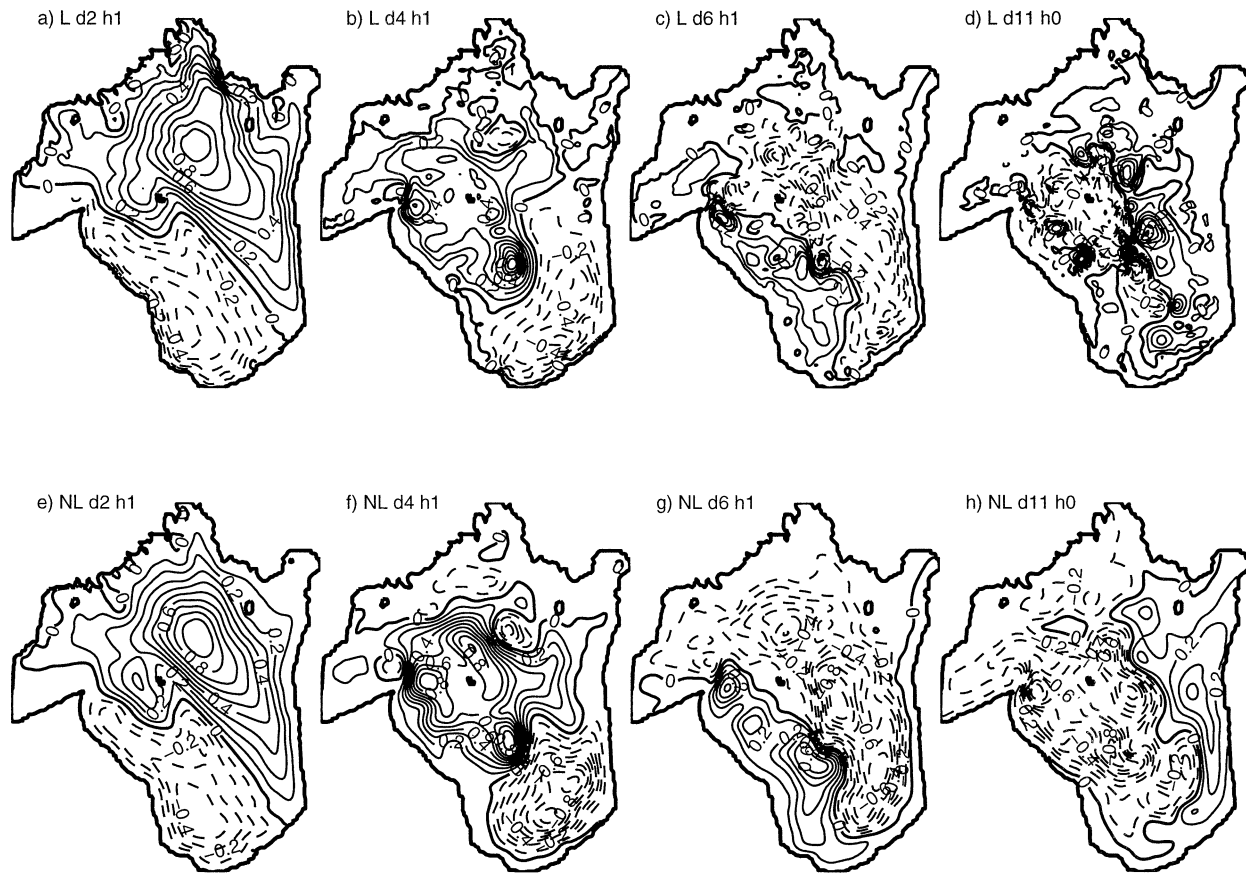
FIG. 2. Normalized streamfunction in response to the impulse-type wind from NW: (a)–(d) linear model and (e–h) nonlinear model. Model simulations started on day 1 hour 0.

is approximated by a linear drag law. The effect of tides is negligible in the Baltic Sea (Mälkki 1975) and was not included in model simulations.

The hydrodynamic models of the Gulf of Riga have uniform horizontal grid size of 1 km. The 3D model has 20 vertical layers. Mean sea level of 1 m is added to avoid drying of the shallow area during storms, which otherwise may cause the model to blow up.

3. Basin-scale topographic wave structure: Linear versus nonlinear response

The initiation of the circulation in the Gulf of Riga due to suddenly imposed wind stress and its subsequent evolution after the wind forcing is removed is investigated by both linear and nonlinear 2D numerical models. Both models are forced by an idealized impulse-type wind from the northwest, which approximately coincides with the orientation of the main topographic features of the basin. The wind stress increases linearly from zero to its maximum value (0.4 N m^{-2}) over 18 h, remains constant at this maximum value for another 6 h, and then decreases linearly to zero during the next 5 h. The wind forcing then remains at zero for the duration of model simulation (10 days).

Normalized transport streamfunctions are shown in Figs. 2a and 2e after 25 h from the imposition of wind. This time instant still corresponds to a relatively strong wind forcing. The double-gyre structure that represents the gravest mode basin-scale topographic wave (Lamb 1932; Ball 1965; Saylor et al. 1980; Bennett and Schwab 1981) is well developed.

The cyclonic gyre has formed over the southwest part of the basin and the anticyclonic gyre is apparent over the northeast part of the basin. Downwind flow has been established along the western and eastern shores and return flow over the central part of the basin. Small deflections of the gyres from a two-gyre pattern are due to the irregular shape and bottom topography of the Gulf of Riga. Because of the island in the center of the basin, the return flow is split into two branches on both sides of the island. An anticyclonic eddy to the west of the island develops due to wind-forced currents over local bottom topography.

Both models produce similar circulation patterns (Fig. 2). Still there are several differences that are clearly brought up by nonlinearity and horizontal diffusion. The streamlines are packed closer to the coast in the linear model. This indicates stronger currents over the shallow area and enhanced differences of the longshore velocity
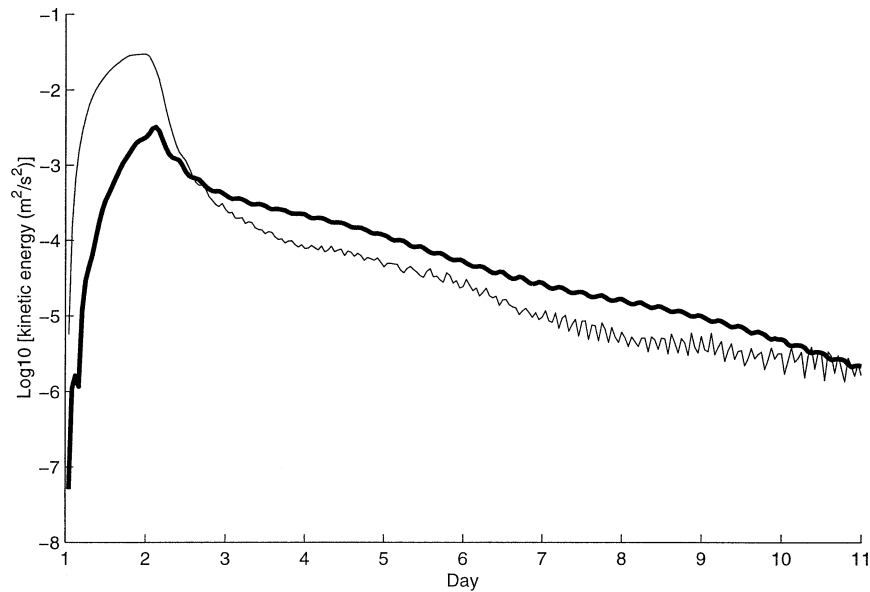
FIG. 3. Time series of mean kinetic energy from the nonlinear numerical model experiment with NW wind impulse. The lines correspond to regions where water depth is between 0 and 9 m (thin) and between 40 m and maximum depth (bold).

between coastal and offshore areas. The eddy west of the central island is more pronounced in the nonlinear model response.

The circulation pattern propagates cyclonically completing a half cycle in 4 days. At this rate, the period of the topographic wave would be 8 days. However, dissipation by bottom friction begins to slow the wave down and decrease the amplitude so that it is difficult to track after 4 days. The double-gyre structure has been retained in a basin-scale sense, with dominant cyclonic circulation over the northeast part of the basin and anticyclonic circulation over the southwest part of the basin. Locally, a number of small-scale circulation cells have been formed. Compared to the initial circulation structure, which was dominated by the first basin-scale topographic mode, the contribution from higher modes has been increased. The differences between the linear and nonlinear model are more pronounced. At the end of the simulation (day 11), the circulation has become predominantly cyclonic in the nonlinear model compared to the linear model (Figs. 2d,h) (e.g., Simons 1986).

Relatively fast dissipation of the flow due to bottom friction is corroborated by calculating mean kinetic energy over different depth intervals. Mean kinetic energy over the shallow area (0–9 m) and deep area ($\geq$40 m) were compared (Fig. 3). During the forcing period, the wind drives stronger currents over the shallow area than over the deep area. The difference between levels of mean kinetic energy is about an order of magnitude. After the forcing is removed, the kinetic energy decreases rapidly over the shallow area. The most significant decrease occurs within a day after the removal of the forcing. Then mean kinetic energy drops more than

two orders of magnitude over the shallow area and about an order of magnitude over the deep area, so that mean kinetic energy over the deep area becomes higher than over the shallow area.

The free topographic wave does not complete a full cycle due to the shallowness of the Gulf of Riga. Even so, the remnants of the gravest mode topographic wave can be identified at the end of the simulation. Variations of the bottom friction coefficient within reasonable limits does not change the results qualitatively.

4. Comparison of model results with observations

The hydrodynamic model was applied with realistic wind for a 45-day period (1 June–17 July 1994). The model was forced by horizontally uniform but temporally variable wind (Fig. 4), which was measured at an island-based meteorological station. The station is a little bit outside of the basin's area, but is less influenced by coastal irregularities, from which the wind around the basin's perimeter should suffer. The use of wind data from a single station is justified by the fact that typical synoptic-scale atmospheric disturbances cover a larger area than the Gulf of Riga. Moreover, the wind data used were corroborated by the wind observations at two other meteorological stations in the northeastern and northern part of the gulf. The wind record consists of wind speed and direction measured at 6-h intervals, potentially aliasing the higher-frequency ($<$12 h period) part of the wind forcing. However, since the characteristic response period of the gulf to wind forcing is several days, this would not affect the results essentially.
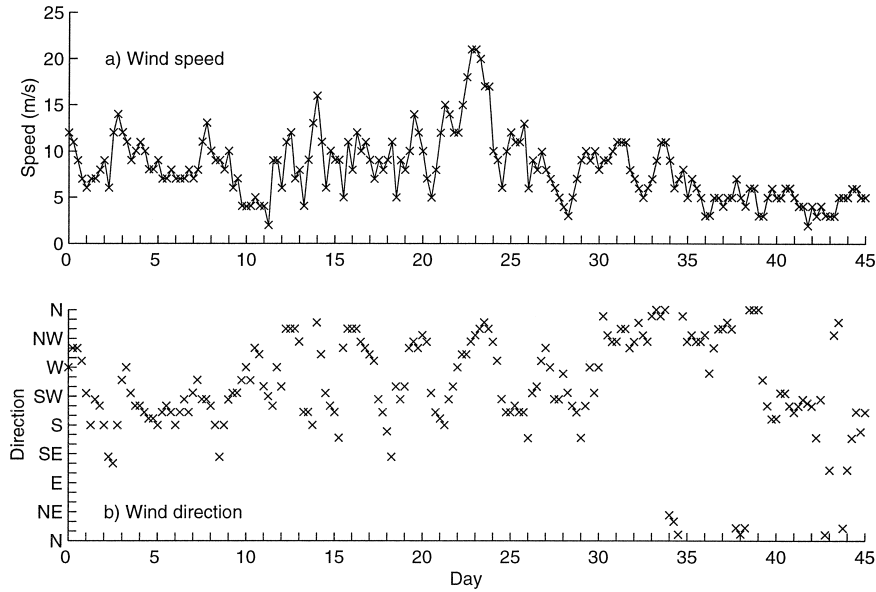
FIG. 4. Measured (a) wind speed and (b) direction. Day 0 corresponds to 1 Jun 1994.

Wind speed was converted to wind stress assuming neutral stability of the atmospheric boundary layer.

In order to test the validity of the numerical model, model results are compared to observations from a current meter mooring which was deployed in the central Gulf of Riga (57°35.5′N, 23°37.1′E) in 54 m of water during a 3-week period in June 1994 (Fig. 1). The mooring consisted of two current meters attached to a cable at 50 and 52 m. The differences of the currents between the current meters were marginal—that is, the mean current speeds are 0.071 and 0.067 m s^{-1} at 50 and 52 m, respectively, and the correlation coefficients are 0.91 and 0.93 for the east and north velocity component, respectively (Raudsepp and Kõuts 2001). The model currents were compared with both current meter data records with similar results. Only the 52-m current meter is presented in the model comparison.

Time dependent model currents are compared with measured currents for three different model configurations: the 1) 2D model (nonlinear), 2) 3D barotropic model (zero stratification), and 3) 3D baroclinic model. Temperature and salinity fields for the baroclinic model were prepared based on the climatological June temperature and salinity profiles in the Gulf of Riga (Raudsepp 2001). The temperature field varied only in the vertical, while both vertical and horizontal salinity variations were included. The model was run for 10 days in the diagnostic mode (temperature and salinity fields kept fixed) to generate steady baroclinic currents in the absence of wind. The wind forcing was applied on 1 June (model day 0) while the salinity and temperature fields were kept fixed throughout the model run.

The depth-averaged currents are compared with the measured currents for the first case (2D model). In the other cases (3D models), the modeled 3D currents were

used (Fig. 5). The 2D model yields results in agreement with the measurements. The 3D models provide only marginal improvement. Comparative tests by the barotropic model with depth-dependent bottom roughness,

$$z_b = 0.002\left(1 + \frac{20}{h}\right),$$

where h is depth, and by the prognostic model (prognostic equations for temperature and salinity were implemented) did not show any significant improvement. The model results indicate the dominance of wind-forced currents in the Gulf of Riga during this period. In the following sections, only the 2D model results are used.

5. Discussion

a. Basin-scale vorticity dynamics

Topographic waves belong to the so called vorticity wave class (Longuet-Higgins 1968; Rhines 1969). Therefore, we use the vorticity equation instead of momentum and continuity equations to analyze the dynamics of the topographic wave response. The vorticity equation for vertically averaged flow in response to spatially uniform wind is

$$\underbrace{\frac{\partial}{\partial t}\zeta}_{\text{I}} + \underbrace{\mathbf{u} \cdot \nabla\zeta}_{\text{IIa}} - \underbrace{\frac{\zeta}{h}(\mathbf{u} \cdot \nabla h)}_{\text{IIb}} - \underbrace{\frac{f}{h}\mathbf{u} \cdot \nabla h}_{\text{III}}$$

$$= \underbrace{\frac{1}{h^2}\mathbf{k} \cdot \left(\frac{\boldsymbol{\tau}_w}{\rho}\right) \times \nabla h}_{\text{IV}} - \underbrace{\mathbf{k} \cdot \nabla \times \left(\frac{\boldsymbol{\tau}_b}{\rho h}\right)}_{\text{V}} + \underbrace{\mathbf{k} \cdot \nabla \times \mathbf{G}}_{\text{VI}},$$
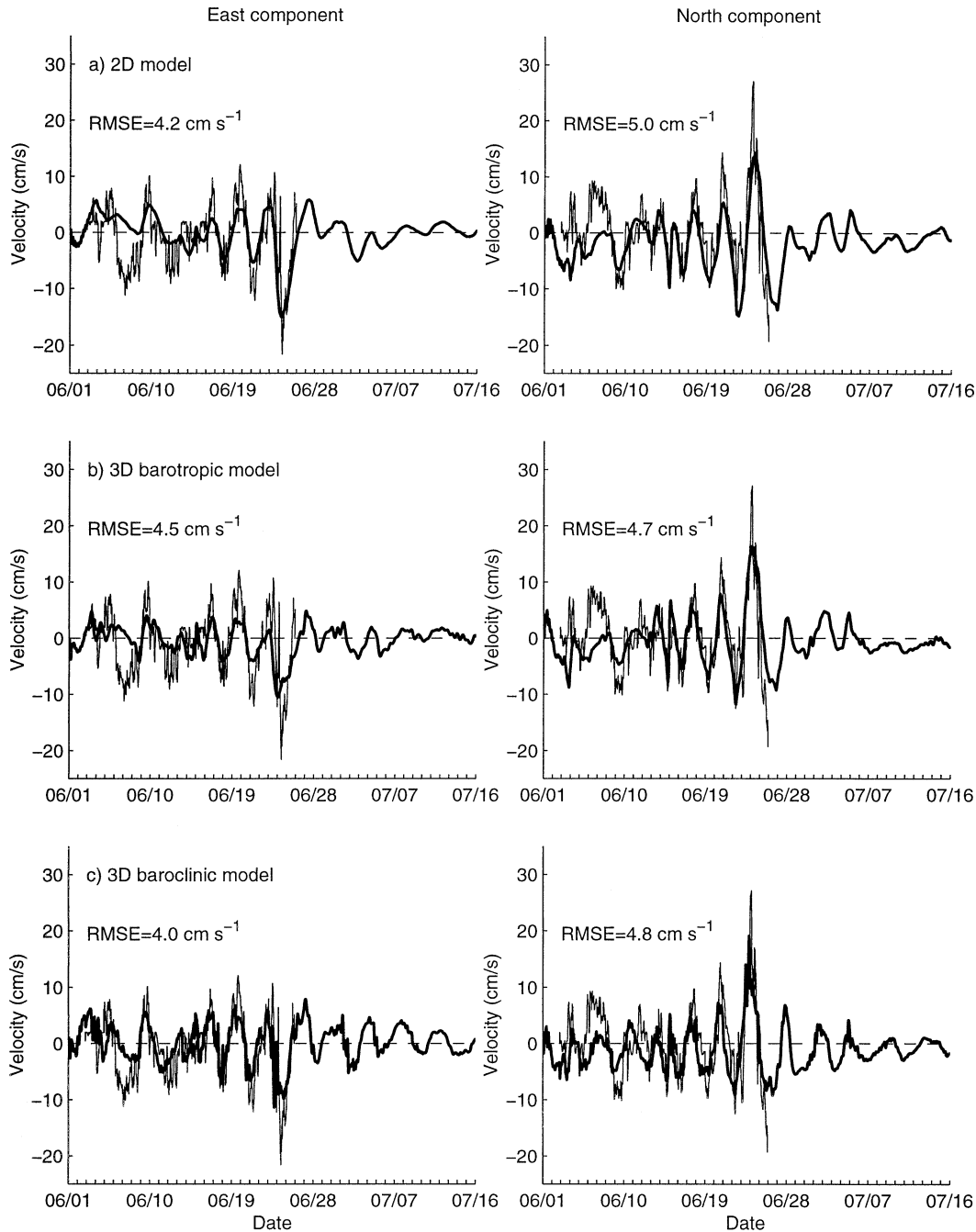
(1)

FIG. 5. Observed [point P1 (thin)] and modeled (bold) east and north velocity components: (a) 2D model (depth-averaged model currents are compared with measured currents at depth 52 m), (b) 3D barotropic model (model currents at 52.5-m depth level are compared with measured currents at 52 m), and (c) 3D baroclinic model (model currents at 52.5-m depth level are compared with measured currents at 52 m).

where ζ is relative vorticity; $\mathbf{u}$ is depth-averaged velocity; h is depth; f is the Coriolis parameter; $\boldsymbol{\tau}_w$ and $\boldsymbol{\tau}_b$ are wind and bottom stress, respectively; $\mathbf{k}$ is the vertical unit vector; ρ is the reference density; and $\mathbf{G}$ is implicitly written horizontal diffusion.

The vorticity [term I in (1), "vorticity tendency"] is generated by the wind stress component perpendicular

to the depth gradient [term IV in (1), "bottom slope vorticity"; Weenink (1958) referred to the water circulation excited by spatially uniform wind stress perpendicular to the depth gradient as a "bottom slope current"]. The vorticity pattern will propagate cyclonically around the basin in the form of a vorticity wave due to Earth's rotation [term III in (1), "wave vortici-
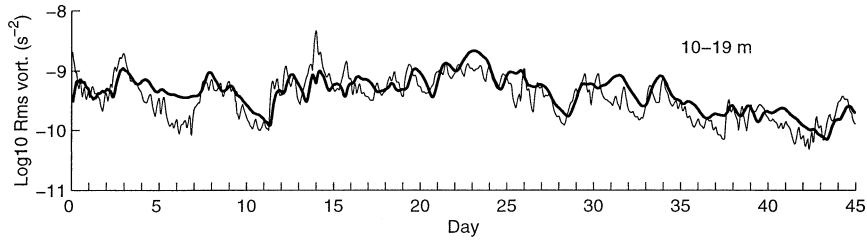
FIG. 6. Rms value of wave vorticity (bold) and vorticity tendency (thin) for region where water depth is 10–19 m. Day 0 corresponds to 1 Jun 1994.

ty"]. The terms I and III form the equation for the free topographic waves. The wave will be dissipated by bottom friction [term V in (1), "friction vorticity"] and horizontal diffusion [term VI in (1), "vorticity diffusion"], and will be modified by nonlinear topographic wave interactions [terms IIa and IIb in (1), "nonlinear vorticity"].

The basin-scale dynamics are investigated by estimating the relative importance of the terms in (1). To estimate relative values, the root-mean-square (rms) value for each term was calculated. The basin is separated into five regions according to the basin's depth in the intervals: 0–9, 10–19, 20–29, 30–39, 40–max(h). The vorticity tendency and wave vorticity should represent topographic wave response. The time series of these terms are presented in Fig. 6 for the depth range of 10–19 m. The wave vorticity and vorticity tendency compare reasonably well for this depth range and others (not shown), except for short-term (>1 cpd) fluctuations. Time series of four terms in (1), wave vorticity, bottom slope vorticity, friction vorticity, and nonlinear vorticity, for each region and also for the whole basin are shown in Fig. 7. The values of the terms vary over several orders of magnitude. The average magnitudes of the terms was estimated by calculating the means of $\log_{10}$ of rms of different terms in (1). Vorticity diffusion was lower than the other terms in (1) for each region and is neglected in the analysis.

The values calculated over the shallow area are about two orders of magnitude higher than the values calculated over the deeper area. Because of that, the variations of the vorticity terms for the whole basin resemble the variations in the shallow area. In the depth range of 0–9 m, bottom slope vorticity dominates other terms. It is not canceled entirely by the friction vorticity. The wave vorticity and nonlinear vorticity are at least one order of magnitude smaller than the other two terms. Also, vorticity dissipation is too low to balance the bottom slope vorticity. Therefore, relative vorticity changes locally according to the wind and the topographic wave is practically absent.

The direct effect of wind and the role of friction vorticity decreases while the importance of wave vorticity and nonlinear vorticity increases with the basin's depth. Still, over the shallow area (depth 10–19 m) the main balance is between bottom slope vorticity and friction

vorticity. Especially during moderate and strong winds, the bottom slope vorticity is balanced by friction vorticity due to the flow along the depth contours in the direction of wind

$$0 \cong \frac{1}{h^2}\mathbf{k}\cdot\left(\frac{\boldsymbol{\tau}_w}{\rho}\right)\times\boldsymbol{\nabla}h - \frac{1}{h^2}C_b|\mathbf{u}|\mathbf{k}\cdot\mathbf{u}\times\boldsymbol{\nabla}h. \quad (2)$$

The magnitude of the sum of bottom slope vorticity and friction vorticity, as these terms balance each other, compares with the magnitude of wave vorticity (Fig. 8) and vorticity tendency (Fig. 6). Dynamically, this is the region of strong influence of the topographic wave (the absolute magnitude of the wave vorticity is considerably higher in the shallow area than in the deeper area). This phenomenon, where wind forcing is balanced by bottom friction to the first order, while the residual of the sum of these terms and the topographic wave terms give the next order balance, may be called the "hidden topographic wave." Thus, the topographic wave response is scarcely observed over the depth range of 10–19 m, which agrees with the result by Hickey (1981) on the continental shelf.

All terms have comparable magnitude between 20- and 29-m depth (Fig. 7). The response consists of a combination of the forced and free wave. During moderate and strong winds the forced response dominates, while during calm periods, when it is preceded by strong wind, the response should resemble the free wave. For the regions deeper than 30 m, the friction vorticity is negligible, except during the storms. The balance is between vorticity tendency and wave vorticity, only moderate and strong wind events have a direct effect on the wave. There, the model results and the measurements show preferred cyclonic rotation of the velocity vector, which is consistent with the dominant basin-scale topographic wave. Changes in the sense of rotation of wind direction do not reverse the sense of rotation of the velocity.

Wave vorticity and nonlinear vorticity follow each other rather closely (Fig. 7). All terms follow bottom slope vorticity in the shallow area, that is, in the region of direct wind effect. In the deep area ($h \geq 30$ m), the wave vorticity and nonlinear vorticity differ from the bottom slope vorticity considerably. The disparity of the variations of nonlinear vorticity and bottom slope vor-
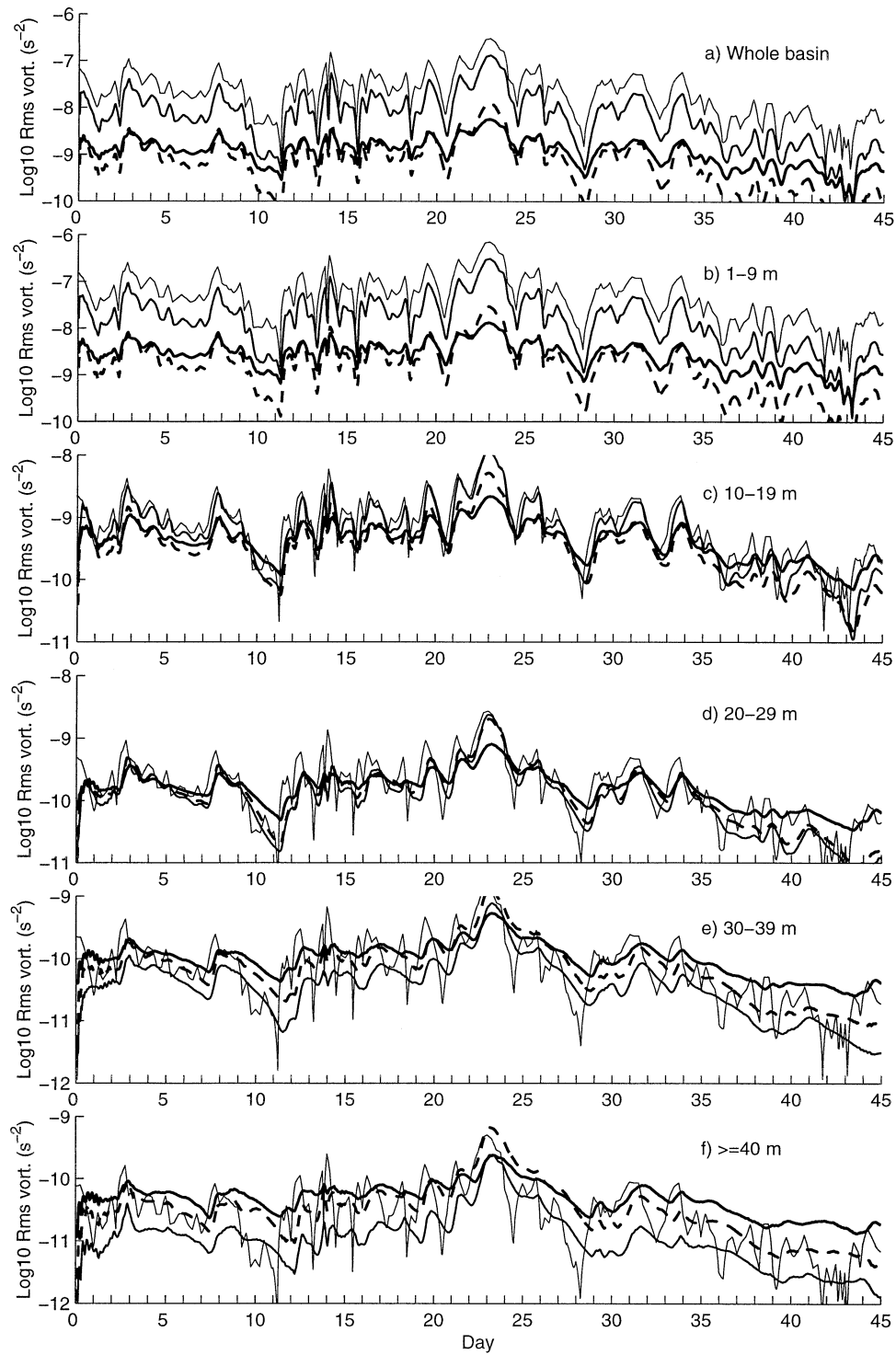
FIG. 7. Rms value of wave vorticity (bold), friction vorticity (regular), bottom slope vorticity (thin), and nonlinear vorticity (dashed) for (a) whole basin, (b) region where water depth is 1–9 m, (c) 10–19 m, (d) 20–29 m, (e) 30–39 m, and (f) ≥40 m. Day 0 corresponds to 1 Jun 1994.
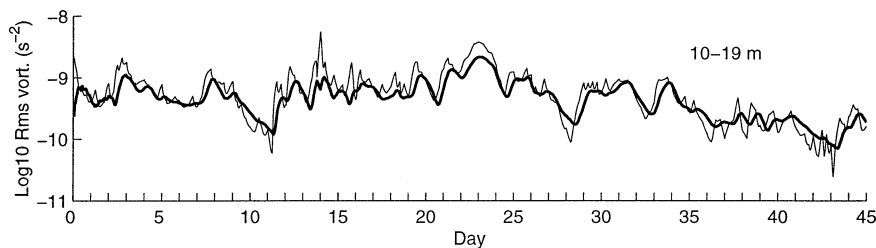
FIG. 8. Rms value of wave vorticity (bold) and the sum of bottom slope vorticity and friction vorticity (thin) for a region where water depth is 10–19 m. Day 0 corresponds to 1 Jun 1994.

ticity increases during low winds and emerges over more shallow areas. During strong winds nonlinear vorticity follows the changes of bottom slope vorticity much closer, even over the deep area. The wave vorticity has a higher value than nonlinear vorticity most of the time, both terms are in phase, while having phase shift with bottom slope vorticity. The above arguments indicate that nonlinear processes are associated with topographic waves, especially during low winds and over the deep area.

b. Topographic wave dynamics in the presence of rotating wind

The wind effect on generation and evolution of the basin-scale topographic wave is shown for the period of days 16–20 (Fig. 9). Wind speed was about 10 m s^{-1} without significant changes. The topographic mode structure is established for day 16.5 after one day of NW wind. The wind destroyed the previous topographic wave structure and the new structure resembles the topographic mode structure generated by impulse-type wind. Between day 16.5 and 17.5, the wave has propagated cyclonically about one-eighth of a cycle. The wind was turning slowly from NW to SW being mostly in phase with the wave. Between day 17.5 and day 18.25, the wind turned from SW to SE and then, between day 18.25 and 18.5, rapidly back to SW. During the first period the wind changed direction faster than the topographic wave. Between day 17.5 and 18.5, the wave has propagated one-quarter cycle, which is twice the phase propagation between day 16.5 and 17.5. The basic double-gyre structure is maintained well. The anticyclonic eddies over the area to the west from the island are the result of wave scattering over local bottom topography. The circulation structure corresponds to the unforced response 4 days after the wind forcing was removed (Fig. 2g). The forced topographic wave has propagated faster than the free wave, that is, 1/4 cpd (Figs. 9a,c) and 1/8 cpd (Figs. 2e,g), respectively. Cyclonically rotating wind, that changes direction faster than the wave, increases the apparent phase speed of the wave. Since day 18.5, the wind, as it turns anticyclonically from SW to NW, acts to destroy the existing wave, and the wave structure has been destroyed by day 19.5. The remnants of the topographic mode can be

identified in the central area of the gulf in the form of a dipole eddy—the cyclonic part on the north and anticyclonic part on the south (Fig. 9d). There, the wind-forcing term is relatively small due to large depth, while the wave term is locally large because of large bottom gradient. The new wave structure emerged on day 20, similar to the one on day 16.5. Subsequently, this topographic wave evolution was repeated under the influence of similar forcing. Overall, cyclonically rotating wind appears to support the topographic wave (from day 16.5 to 18.5), while anticyclonically rotating wind tends to destroy the existing wave structure (from day 18.5 to 19.5).

c. Topographic wave dynamics in response to weak wind

The nonlinear model simulation showed that the double-gyre circulation evolves slowly into a predominantly cyclonic vortex after the wind forcing is removed (section 3). Because the wind never ceases for a sufficiently long time during the realistic case simulation, there is no period when unforced propagation of the topographic wave could be examined. The closest approximation to this condition would be to examine the propagation and evolution of the topographic mode structure under the weak wind conditions (days 39–44). The wind speed was about 5 m s^{-1} and the wind direction changed cyclonically during this period, which should support the double gyre pattern. In general, the current velocities were also low (<5 cm s^{-1}, except in the coastal area). The sequence of streamfunction patterns is presented in Fig. 10. The streamfunction patterns represent a double-gyre structure in a basin-scale sense. Locally, there are a number of eddies both cyclonic and anticyclonic that dominate in the velocity field. Still, the basin-scale streamfunction pattern propagates cyclonically and completes about half of a cycle in 3 days, from day 39 to day 42. Thus, the propagation speed is higher than in unforced case because even the weak wind occasionally affects the wave in the area where basin is shallower than 30 m (Fig. 7). Similar to the model experiment with impulse-type wind, the circulation becomes more cyclonic under the weak wind forcing. In the velocity field, there are many small-scale eddies, but
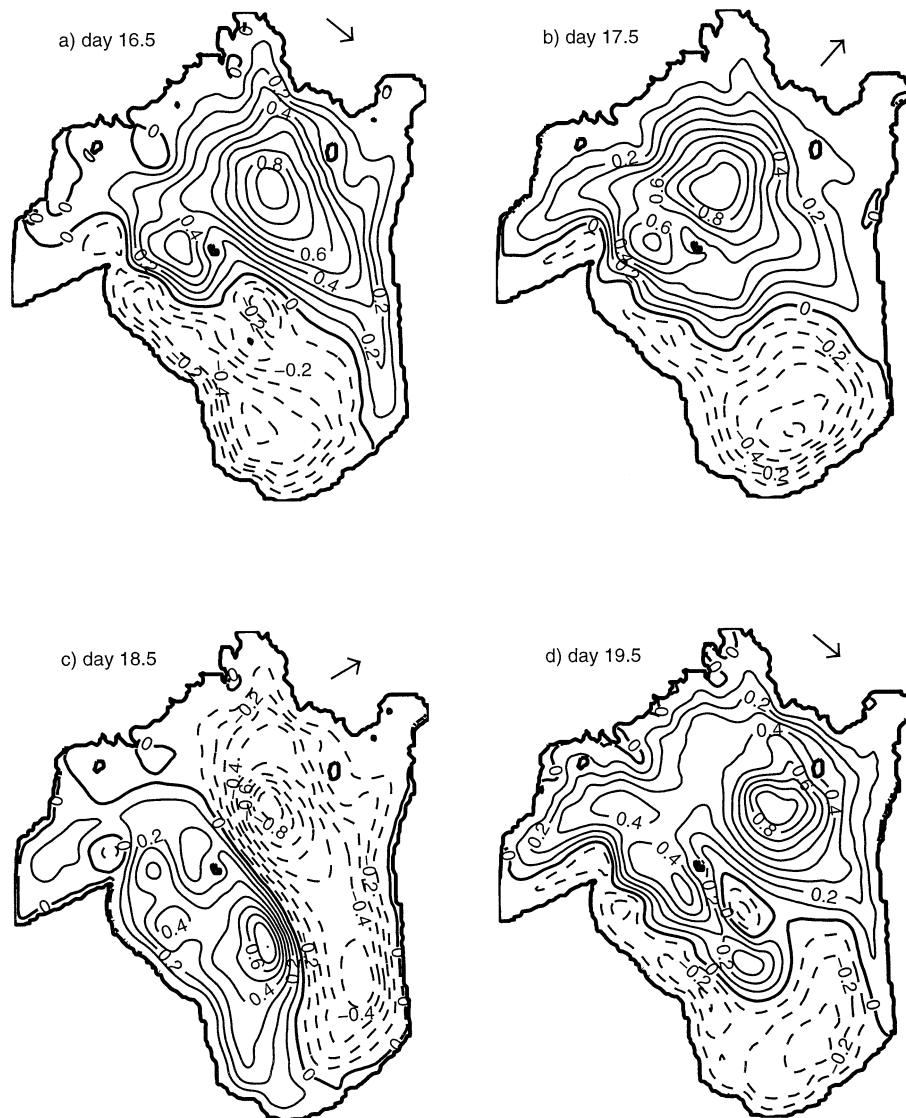
Fig. 9. Normalized streamfunction on day (a) 16.5, (b) 17.5, (c) 18.5, and (d) 19.5. Day 0 corresponds to 1 Jun 1994. Bold arrow shows the direction of the wind.

in general they contribute to the cyclonic circulation pattern.

6. Conclusions

A barotropic two-dimensional model was used to study the basin-scale circulation in the Gulf of Riga, forced by spatially uniform wind measured at 6-h time intervals. The model can accurately simulate low-frequency observed current variability in the central Gulf of Riga even with the straits being closed. More sophisticated models—3D barotropic and baroclinic models—produce only marginal improvement.

The model simulation proves the hypothesis that observed low-frequency current variations can be explained by basin-scale topographic wave. The response

to a spatially uniform wind consists of double-gyre circulation pattern that resembles the gravest mode basin scale topographic wave. Moderate and strong winds of about 1-day duration are sufficient to change the existing circulation pattern and to establish a new basin-scale topographic wave structure. The free topographic wave propagates cyclonically around the basin. Using basin-scale vorticity dynamics it was shown that in very shallow areas (depth less than 10 m) the topographic wave is absent. In areas shallower than 20 m, the free topographic wave is easily destroyed because of the dominance of direct wind forcing and bottom friction in the vorticity balance. The wave survives in the deep area where the direct wind effect is much smaller compared to other terms. The Gulf of Riga is relatively shallow so that a free basin-scale topographic wave is signifi-
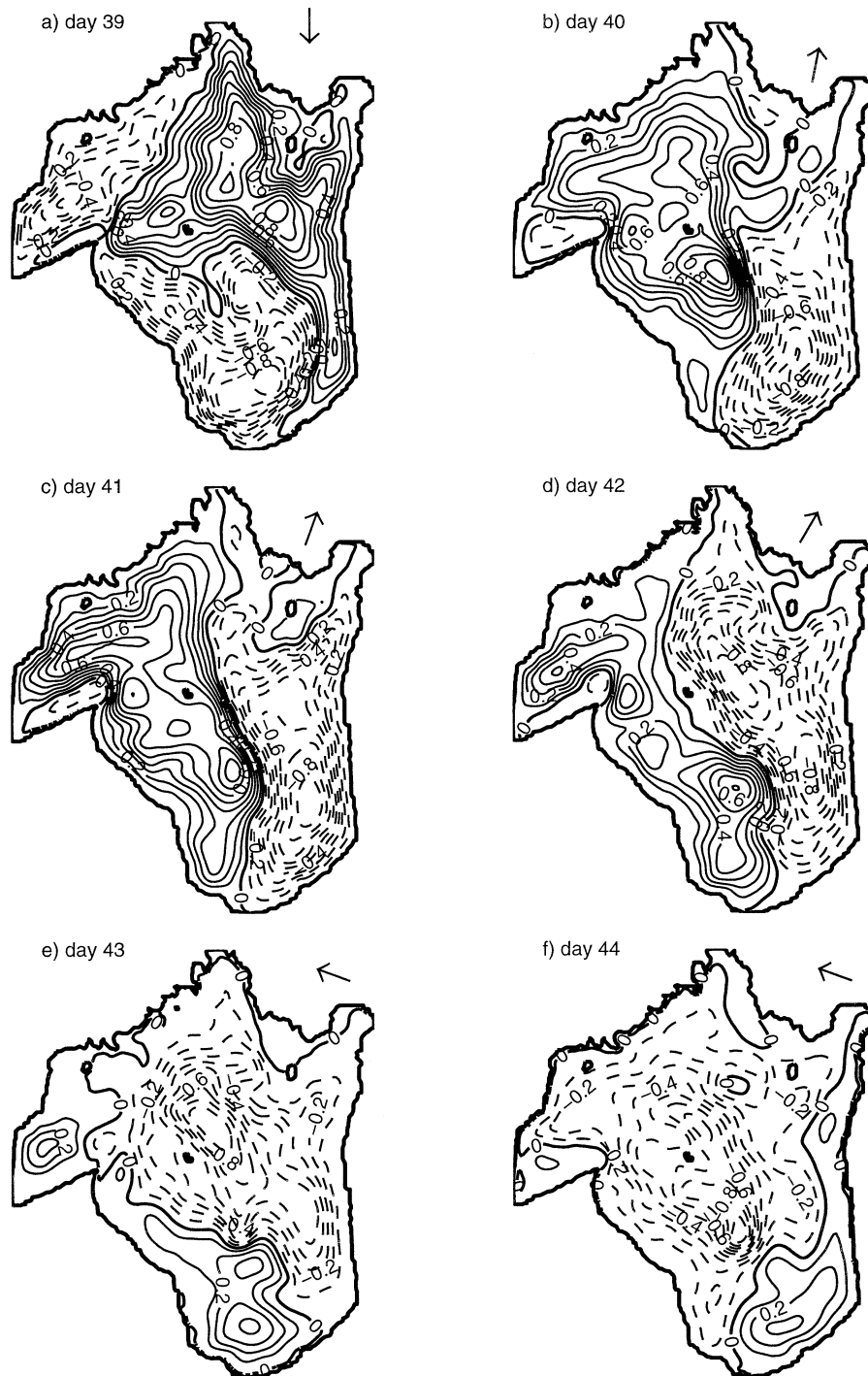
FIG. 10. Normalized streamfunction on day (a) 39, (b) 40, (c) 41, (d) 42, (e) 43, and (f) 44. Day 0 corresponds to 1 Jun 1994. Bold arrow shows the direction of the wind.

cantly distorted and does not complete a full cycle. Also, higher modes of the basin-scale topographic wave will contribute to the overall circulation field. If the wind varies in time, then the temporal evolution of the flow field consists of the combined effects of the free wave and wind-forced response. Cyclonically rotating wind can reinforce the basin-scale topographic wave. If the wind changes direction faster than the topographic wave, then the apparent phase speed of the wave increases compared to the free wave. Anticyclonically rotating wind tends to destroy the wave. During calm periods or under the influence of weak winds, the dou-

ble-gyre circulation will evolve into predominantly cyclonic circulation. This phenomenon occurs only in the nonlinear model simulations and therefore is essentially nonlinear.

REFERENCES

Ball, F. K., 1965: Second-class motions of a shallow liquid. *J. Fluid Mech.,* **23,** 545–561.

Bennett, J. R., 1974: On the dynamics of wind-driven lake currents. *J. Phys. Oceanogr.,* **4,** 400–414.

——, and D. J. Schwab, 1981: Calculation of the rotational normal modes of oceans and lakes with general orthogonal coordinates. *J. Comput. Phys.,* **44,** 359–376.

Blumberg, A. F., and G. L. Mellor, 1987: A description of a three-dimensional coastal ocean circulation model. *Three-Dimensional Coastal Ocean Models, Coastal and Estuarine Sciences,* N. S. Heaps, Ed., Vol. 4, Amer. Geophys. Union, 1–16.

Csanady, G. T., 1974: Reply. *J. Phys. Oceanogr.,* **4,** 271–273.

Hickey, B. M., 1981: Alongshore coherence on the Pacific Northwest continental shelf, January to April, 1975. *J. Phys. Oceanogr.,* **11,** 822–835.

Lamb, H., 1932: *Hydrodynamics.* Dover, 738 pp.

Longuet-Higgins, M. S., 1968: Double Kelvin waves with continuous depth profiles. *J. Fluid Mech.,* **34,** 49–80.

Mälkki, P., 1975: On the variability of currents in a coastal region of the Baltic Sea. *Merentutkimuslaitoksen Julk.,* **240,** 3–56.

Mellor, G. L., and T. Yamada, 1982: Development of a turbulence closure model for geophysical fluid problems. *Rev. Geophys. Space Phys.,* **20** (4), 851–875.

Rao, D. B., and D. J. Schwab, 1976: Two-dimensional normal modes in arbitrary enclosed basins on a rotating earth: Application to Lakes Ontario and Superior. *Philos. Trans. Roy. Soc. London,* **A281,** 63–96.

Raudsepp, U., 2001: Interannual and seasonal temperature and salinity variations in the Gulf of Riga and corresponding saline water inflow from the Baltic Proper. *Nordic Hydrol.,* **32,** 135–160.

——, and T. Kõuts, 2001: Observations of near-bottom currents in the Gulf of Riga, Baltic Sea. *Aquat. Sci.,* **63,** 385–405.

Rhines, P. B., 1969: Slow oscillations in an ocean of varying depth. *J. Fluid Mech.,* **37,** 161–205.

Saylor, J. H., J. C. K. Huang, and R. O. Reid, 1980: Vortex modes in southern Lake Michigan. *J. Phys. Oceanogr.,* **10,** 1814–1823.

Schwab, D. J., 1983: Numerical simulation of low-frequency current fluctuations in Lake Michigan. *J. Phys. Oceanogr.,* **13,** 2213–2224.

Simons, T. J., 1975: Verification of numerical models of Lake Ontario. Part II: Stratified circulation and temperature changes. *J. Phys. Oceanogr.,* **5,** 98–110.

——, 1983: Resonant topographic response of nearshore currents to wind forcing. *J. Phys. Oceanogr.,* **13,** 512–523.

——, 1986: The mean circulation of unstratified bodies driven by nonlinear topographic wave interaction. *J. Phys. Oceanogr.,* **16,** 1138–1142.

Smagorinsky, J., 1963: General circulation experiments with the primitive equations. *Mon. Wea. Rev.,* **91,** 91–164.

Stocker, T., and K. Hutter, 1987: Topographic waves in channels and lakes on the f-plane. *Lecture Notes on Coastal and Estuarine Studies,* Vol. 21, Springer, 176 pp.

Weenink, M. P. H., 1958: A theory and method of calculation of wind effects on sea levels in a partly enclosed sea. Royal Netherlands Meteorological Institute, Mededeelingen en verhandelinden 73, 111 pp.